AGU PUBLICATIONS

Geophysical Research Letters

RESEARCH LETTER
10.1002/2017GL075930

Special Section:
Midlatitude Marine Heatwaves: Forcing and Impacts

Increasing Coupling Between NPGO and PDO Leads to Prolonged Marine Heatwaves in the Northeast Pacific

Youngji Joh[1] and Emanuele Di Lorenzo[1]

[1]School of Earth and Atmospheric Sciences, Georgia Institute of Technology, Atlanta, GA, USA

Abstract The marine heatwave of 2014/2015 in the Northeast Pacific caused significant impacts on marine ecosystems and fisheries. While several studies suggest that land and marine heatwaves may intensify under climate change, less is known about the prolonged multiyear nature (~2 years) of the Northeast Pacific events. Examination of reanalysis products and a 30-member climate model ensemble confirms that prolonged multiyear marine heatwaves are linked to the dynamics of the two dominant modes of winter sea surface temperature variability in the North Pacific, the Pacific Decadal Oscillation (PDO), and the North Pacific Gyre Oscillation (NPGO). Specifically, we find a significant correlation between winter warm NPGO anomalies and the following winter PDO arising from extratropical/tropical teleconnections. In the model projections for 2100 under the RCP8.5 scenario, this NPGO/PDO 1 year lag correlation exhibits a significant positive trend (~35%) that favors more prolonged multiyear warm events (>1°C) with larger spatial coverage (~18%) and higher maximum amplitude (~0.5°C for events >2°C) over the Northeast Pacific.

Plain Language Summary Between the winters of 2014 and 2015 the Northeast Pacific experienced the largest and longest marine heatwave ever recorded in the instrumental record. A distinguishing feature of this event is the multiyear persistence of the ocean warm anomalies from one winter to the other. By analyzing and comparing different reanalysis products and an ensemble of climate model projections for 2100, we find that the observational trend for stronger winter to winter persistence of anomalies in the Northeast Pacific is consistent with climate model projections under the RCP8.5 radiative forcing scenario. We link this trend to an increase coupling between the two dominant modes of North Pacific decadal variability.

Key Points:
- Multiyear SST warm events in the Northeast Pacific typically emerge as a winter NPGO-like warm pattern and transition to a PDO-like pattern in the following winter
- The coupling between winter NPGO and the following winter PDO is a robust climate teleconnection in both observations and the CESM-LENS over the period 1920-2100
- A stronger NPGO-PDO coupling is predicted under anthropogenic forcing in the CESM-LENS and leads to more prolonged and larger area multiyear marine heatwaves

Supporting Information:
- Supporting Information S1

Correspondence to:
Y. Joh,
youngji.joh@gmail.com

Citation:
Joh, Y., & Di Lorenzo, E. (2017). Increasing coupling between NPGO and PDO leads to prolonged marine heatwaves in the Northeast Pacific. *Geophysical Research Letters, 44*, 11,663–11,671. https://doi.org/10.1002/2017GL075930

Received 4 OCT 2017
Accepted 8 NOV 2017
Accepted article online 13 NOV 2017
Published online 30 NOV 2017

1. Introduction

The 2013/2015 marine heatwave of the Northeast Pacific was characterized by the strongest ocean temperature extremes ever recorded in the North Pacific (Anderson et al., 2016; Baxter & Nigam, 2015; Bond et al., 2015; Hartmann, 2015; Hobday et al., 2016; Peterson et al., 2016; Wang et al., 2014) and by an unusual persistence that spanned the winters of 2013/2014 and 2014/2015 (Di Lorenzo & Mantua, 2016), culminating in one of the strongest El Niño events of the twentieth century in the fall/winter of 2015/2016. The progression of the event followed distinct spatial and temporal winter patterns in the ocean and atmosphere that closely resemble the two dominant modes of variability of sea surface temperature and sea level pressure anomalies (SSTa and SLPa). Specifically, the spatial structures of the January-February-March (JFM) SSTa in 2013/2014 and 2014/2015 are captured by the 2nd and 1st principal components of the North Pacific SSTa (Di Lorenzo & Mantua, 2016) (Figure S1 in the supporting information). In the Northeast Pacific, these modes are commonly referred to as the North Pacific Gyre Oscillation (NPGO) (Di Lorenzo et al., 2008) and the Pacific Decadal Oscillation (PDO) (Mantua et al., 1997) (Figure S1). The similarity between the marine heatwave patterns and the mode of Pacific decadal variability suggests that the statistics and persistence of these ocean extremes are linked to the dynamics underlying the North Pacific modes.

Using historical reanalysis products and a climate model ensemble, this study provides a diagnostic of ocean extremes statistics in past observations and in future model projections under the radiative forcing scenario RCP8.5. The goal of this study is to (1) confirm the hypothesis that prolonged ocean extremes events follow recurrent patterns with a transition from a winter NPGO-like pattern to PDO-like pattern in the following winter and (2) examine how the coupling between these modes via tropical/extratropical teleconnections is changing under a warmer climate favoring more prolonged winter to winter warm events.

2. Data and Methods

Observations used for investigating the ocean temperature extremes are monthly mean SST data [2° × 2° horizontal grid] of the National Oceanic and Atmospheric Administration Extended Reconstruction SST, version 3 (ERSST.v3) product (Smith et al., 2008) and the Hadley Centre Sea Ice and Sea Surface Temperature (HadiSST) data set (Rayner et al., 2003). For winter extremes, JFM mean SSTa over the Northeast Pacific (20°N–60°N, 170°E–110°E) are used. Anomalies for SST are constructed by removing the mean monthly climatology and linear trend at each grid point. The limited period between 1920 and 2015 is analyzed.

Given that the North Pacific multiyear marine heatwave of 2014/2015 developed initially as a large surface area with anomalously warm SST spanning most of the Northeast Pacific (e.g., the blob), we develop an ocean extreme index (OEI) that is designed to track the occurrence of ocean temperature extremes that cover large areas of the Northeast Pacific [180°E–115°E and 30°N–60°N] (blue box of Figure 1). For a given winter (JFM), we measure the surface area of anomalously warm and cold SSTa that exceed selected thresholds values (1.5°C, 1°C, and 0.5°C), where 0.5°C is the average of standard deviations of SST at all the grid points in Northeast Pacific between 1920 and 2015 (Figures 1a–1c). The red and blue bars indicate the warm and cold water area, respectively. The OEI is then defined by taking the difference of warm minus cold percentage area (black line in Figures 1d and 1e), so that a large positive OEI indicates a winter when most of the Northeast Pacific is covered by surface area with warm SSTa exceeding the selected threshold.

To examine changes in the statistics of ocean temperature extremes under greenhouse forcing, we use the output of the first 30 members of the Community Earth System Model (CESM)-Large Ensemble Community Project (LENS) from 1920 to 2100 under the RCP8.5 greenhouse radiative forcing scenario available at https://www2.cesm.ucar.edu/models/experiments/LENS39 (Kay et al., 2015). Each ensemble member is forced with historical radiative fluxes for the period 1920–2005 and with the RCP8.5 radiative forcing for the period 2006–2100. The CESM-LENS uses a 1° latitude/longitude version of CESM1(CAM5). Prior to analyzing the CESM-LENS data, we remove the warming trends by removing the ensemble mean SST time series at each grid point. This approach to removing the warming trend leads to almost the same results as removing a quadratic trend at each grid point (Figure S6).

In both the observational and model data, we define the first two Empirical Orthogonal Functions (EOFs: computed over the region outlined by the blue box in Figures 1g–1l, the principal components (PC1 and PC2) are then regressed on Northeast Pacific JFM SSTa) as a proxy of the PDO (PC1) and NPGO (PC2) type variability. These modes track closely the spatial and temporal evolution of the record-breaking warm anomalies patterns of JFM 2014 (EOF2) and JFM 2015 (EOF1) (Di Lorenzo & Mantua, 2016).

3. Observed and Predicted Statistics of Ocean Temperature Extremes

To examine the relationship between the modes of the JFM SSTa of the Northeast Pacific (NEP) and the emergence/evolution of marine heatwaves like the 2014/2015, we use the historical reanalyses of SSTa from NOAA ERSSTv3 and HadiSST. Rather than inspecting the statistics of a priori specific SSTa patterns in the data (e.g., PC1 and PC2), we use the OEI to objectively identify the years of emergence of ocean extremes that cover most of the NEP waters like in the winter of 2014—the initiation of the marine heatwave. Inspection of the OEI winter time series (Figures 1d–1f) shows that 2013/2014 and 2014/2015 SSTa emerge as record-breaking warm temperature events independent of the threshold selected in the analysis. A correlation analysis of the OEIs with the dominant modes of NEP JFM SSTa (Figures 1d–1f) confirms a significant correlation (>99% significance, see section 2) with PC2 (e.g., NPGO-like variability) rather than PC1 (e.g., PDO like). Although this result may be expected, given that the NPGO pattern is characterized by a monopole structure in the NEP, it confirms that we can explore the dynamics of the extreme events in the context of the North Pacific modes (e.g., NPGO and PDO). In fact, a correlation of the OEIs with the PC1 (e.g., PDO-like variability) reveals no significant correlations.

To more clearly reveal the spatial patterns associated with these temperature extremes, we perform a composite analysis of winter SSTa when the percent area covered by warm/cold water (Figures 1a–1c) is above the thresholds values of 5%, 15%, and 30%, respectively (Figures 1g–1l). In all threshold cases, warm composites exhibit a large open ocean anomaly in the eastern and central North Pacific resembling the PC2 or

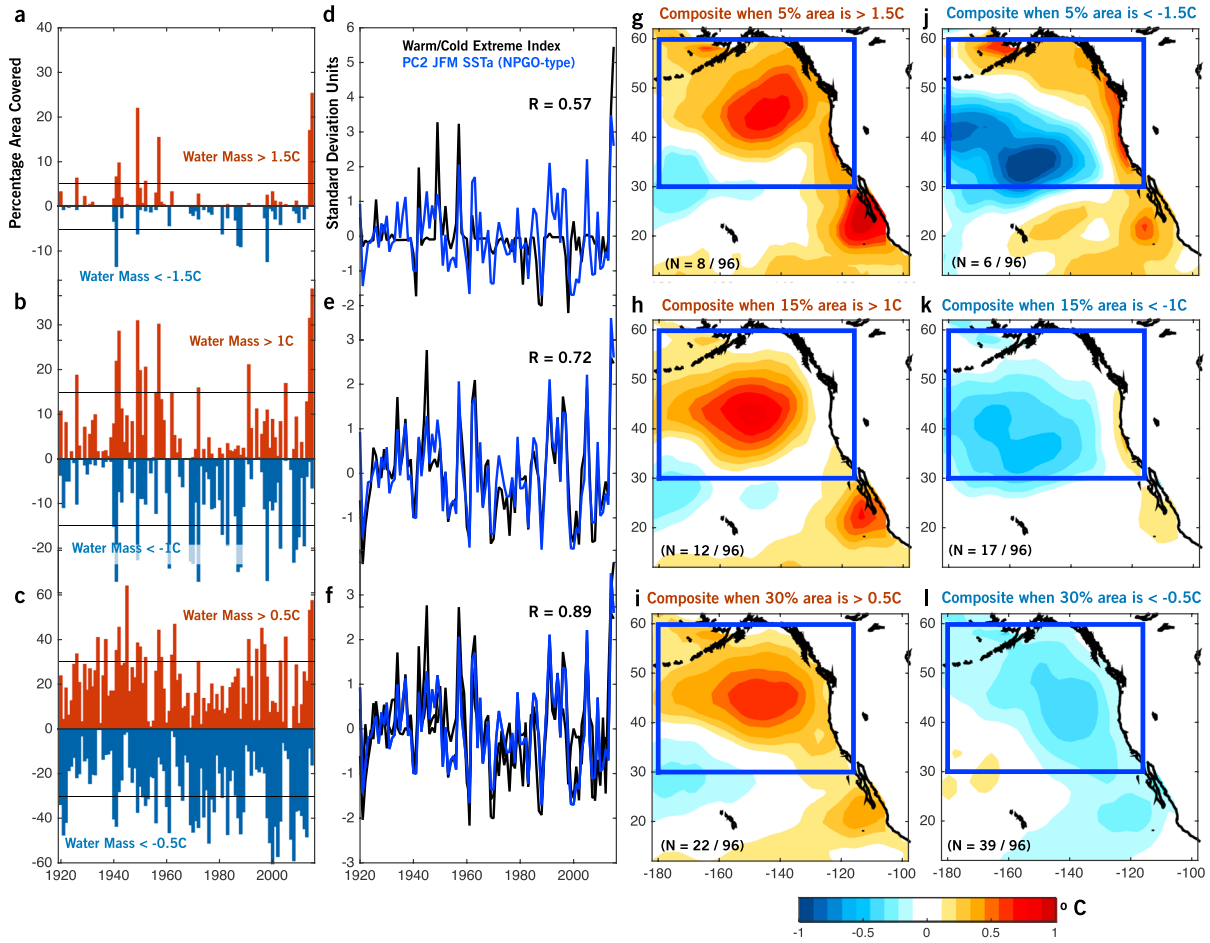

Figure 1. Characteristics of winter ocean temperature extremes in the Northeast Pacific. Percentage of the grid points with anomalously warm (red bars) and cold (blue bars) SSTa of the Northeast Pacific where the JFM SSTa are above the threshold values of (a) 1.5°C, (b) 1°C, and (c) 0.5°C. Corresponding ocean extreme index (OEI) (black) versus PC2 (blue) of JFM SSTa where *R* is a correlation coefficient between the (d–f) OEI and PC2. Composite of JFM SSTa (°C) when the percentage surface areas covered by anomalously warm/cold water with threshold of 1.5°C, 1°C, and 0.5°C exceeds (g, j) 5%, (h, k) 15%, and (i, l) 30%, respectively. Blue box denotes a region used to compute percentage of grid and EOF analysis. Values in parenthesis are the number of events.

NPGO-type expression (Figures 1g–1i), confirming the temporal relationship found between the OEI and the PC2 time series. In contrast, the spatial structures of cold composites demonstrate a more variable pattern that captures both the NPGO and PDO signatures (Figures 1j–1l). For example, the large amplitude cold events (Figure 1j) exhibit a spatial pattern similar to the PDO expression, with negative SSTa in the central Pacific and positive SSTa along west coast of North America. This suggest that warm/cold temperature extremes in the NEP are not symmetric in space and follow different expressions of the dominant modes of the North Pacific decadal variability.

A similar analysis of the OEI is performed on the 30 members of CESM-LENS from 1920 to 2100 forced with the RCP8.5 scenario (see section 2) to explore how robust the characteristics of temperature extremes are in the NEP compared to observations and how they respond to anthropogenic forcing. Prior to the analysis we subtract the ensemble mean SSTa time series at each grid point to remove the warming trend "forced" signal, which would bias the statistics of warm/cold events (Figure S6). The model data are divided into the period of 1951–2000 (hereinafter referred to as the historical simulation) and the period of 2051–2100 (hereinafter referred to as RCP8.5). An inspection of the probability density function (PDF) of the historical and RCP8.5 SSTa over the NEP exhibits overall Gaussian distributions (Figures S2a and S2b). However, a difference of the RCP8.5 minus historical PDF shows a right skewed SSTa distribution in the RCP8.5 indicating an increased (decreased) frequency of warm (cold) temperature anomalies (Figure S2c). This indicates some degree of non-Gaussian behavior in the response of the NEP to anthropogenic forcing, which is likely associated with

the lack of spatial symmetry in the patterns of the warm and cold composites found in both the observations (Figure 1) and in the CESM-LENS (Figures S3 and S4, as discussed below).

Similar to the treatment of the reanalysis products (e.g., Figure 1), we compute warm/cold composites for SSTa thresholds of 0.5°C, 1°C, 1.5°C, and also 2°C to account for the larger number of occurrences of high amplitude events found in the CESM ensemble (e.g., more realizations increase the number of larger extremes counted in the composite, see Figures S3 and S4). Consistent with the observations, both the historical and RCP8.5 warm composites show a preferred monopole pattern resembling the NPGO-like expression, while the cold composites exhibit the hybrid of NPGO-like and PDO-like signatures (Figures S3 and S4). An analysis of the difference in maximum amplitude in the RCP8.5 minus historical composites (Figure S2d) reveals that warm events intensify between 0.3 and 0.5°C and the percentage area covered by surface area with anomalously warm water becomes significantly larger by ~18% (>99% significance) across the different thresholds (Figure S2f). In the frequency statistics, warm events tend to occur slightly more often in the RCP8.5 simulations by ~6% (>99% significance) for 1°C and by ~3% (>95% significance) for 1.5°C cases (Figure S2h). In contrast, differences in cold composites between historical and RCP8.5 show no significant change in the statistics of amplitude or frequency (Figures S2e and S2i) except for the spatial coverage (Figure S2g).

4. Trends of Coupling Between the Dominant Modes of North Pacific Decadal Variability

A distinguishing characteristic of the 2014/2015 NEP marine heatwaves is the multiyear winter to winter prolonged nature of the event (Di Lorenzo & Mantua, 2016) associated with the transition from an NPGO- (2014) to a PDO-like (2015) SSTa expression (Figure S1). We refer to this "prolonged nature" of the event as "persistence" of the warm anomalies, although the spatial pattern is changing as the anomalies transition from an NPGO to PDO-type pattern. This transition is enabled by a two-way coupling between the North Pacific and tropics. Specifically, the NPGO-like winter SSTa pattern in the subtropics activates well-known El Niño precursors dynamics in the spring that energize the growth of El Niño-like tropical SSTa in summer and fall (e.g., Anderson et al., 2013; Vimont et al., 2003). These tropical SSTa activate teleconnections to the extratropic that project onto, and amplify, the PDO-type pattern in the following winter (e.g., Alexander, 1992). These extratropical to tropical teleconnections are a key and dynamically robust mechanism for adding memory and sustaining decadal variance in the Pacific (Di Lorenzo et al., 2015; Di Lorenzo & Mantua, 2016).

To explore how the statistics of winter to winter persistence change over time in the observational record, we use regression maps of the OEI (1°C threshold case) with concurrent and +1 year lag observed SSTa and SLPa evaluated over the periods 1984–2013 and 1951–1983 (Figure 2). In the analysis, we exclude the JFM 2014 and 2015 events so that the statistics are not dominated by the recent large extremes (e.g., the 2014/2015 NEP marine heatwave). The patterns of SSTa and SLPa at lag 0 and +1 year show significant spatial differences. At lag 0 we find the NPGO-like SSTa expression (Figure 2a) and a strong SLPa dipole structure resembling the North Pacific Oscillation (NPO) (Figure 2c). (Chhak et al., 2009; Linkin & Nigam, 2008). At lag year + 1 the PDO-like coastal signature appears along with the El Niño-like pattern in the tropics (Figure 2b). The SLPa also changes to the typical signature of a deepening and shift of the Aleutian Low (Figure 2d). This progression of warm anomaly patterns is consistent with the previous findings related to the 2014/2015 NEP heatwave (Di Lorenzo & Mantua, 2016). By comparing the two periods 1984–2013 (Figure 2, top row) and 1951–1983 (Figure 2, middle row), we find that the multiyear persistence of warm events is more intense in the recent period (Figure 2, bottom row). The atmospheric forcing patterns of the NPO and Aleutian Low become stronger (Figures 2c and 2d) and the tropical footprint of the SSTa (Figures 2a and 2b) more intense. This suggests an increase in persistence associated with stronger tropical/extratropical coupling. More specifically for the recent period 1984–2013, the development of the first winter warm anomalies has a strong subtropical footprint typical of El Niño SSTa and SLPa precursor (e.g., Figure 2a, optimal growth pattern, Penland & Sardeshmukh, 1995; Figure 2c, seasonal footprinting, Vimont et al., 2003). Consistent with these precursor dynamics, the following winter is characterized by a strong El Niño and PDO signatures in the SSTa (Figure 2b) and a more intense Aleutian Low (Figure 2d).

The trend in persistence of marine heatwaves in the NEP is quantified statistically by estimating the winter to winter lag correlation between NPGO- (year 0) and PDO-like (year +1) expressions. The overall

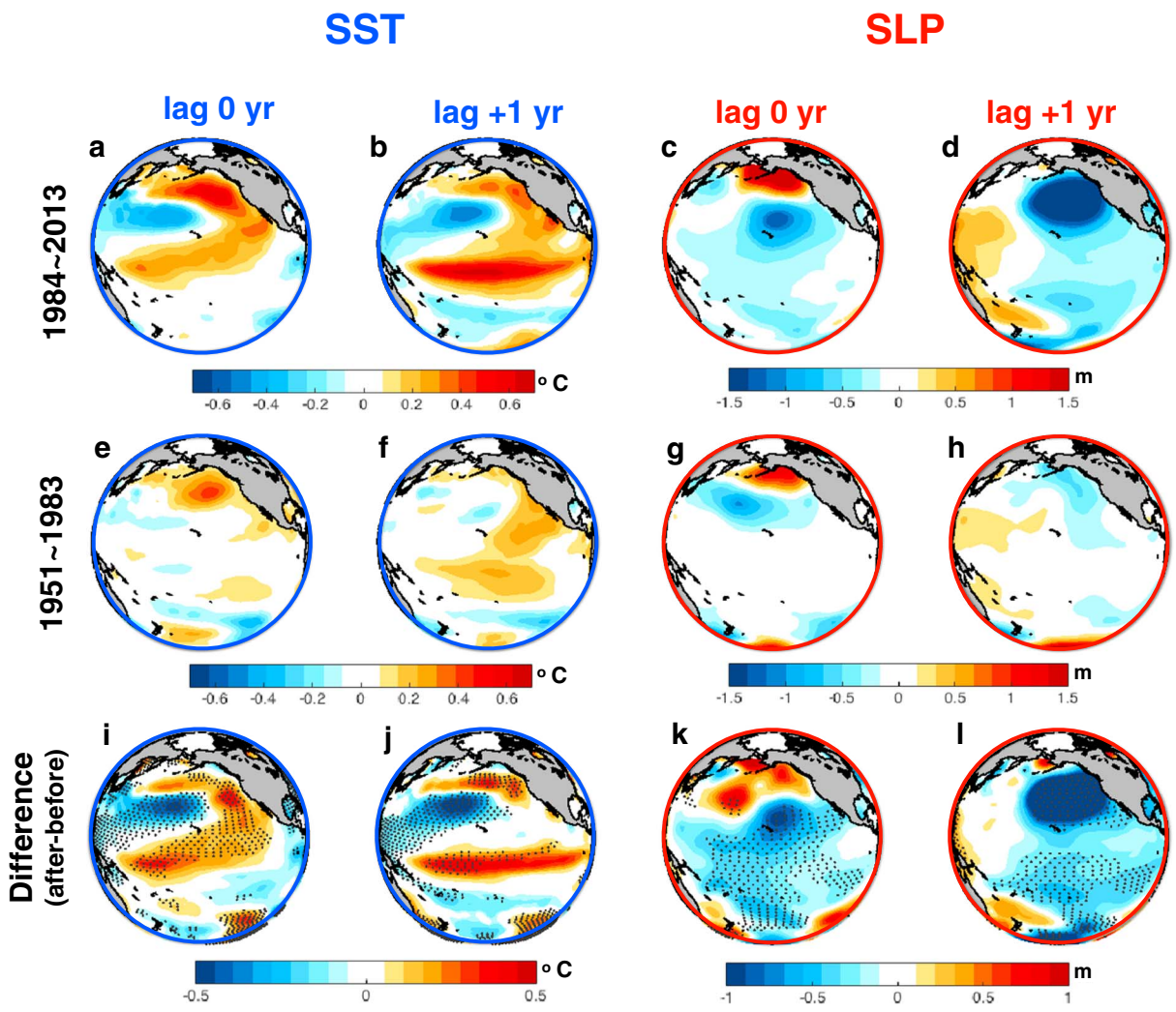

Figure 2. Evolution of observed NEP warm temperature events and related atmospheric forcing. Regression maps of OEI (of 1°C to SSTa and SLPa with 0 and +1 year lag during the period of (a–d) 1984–2013, (e–h) 1951–1983. Difference maps between the (i–l) two periods (recent minus previous). Stippling indicates regions where the difference of two regression coefficients is statistically significant above the 90% confidence level as determined by a two-tailed Student's *t* test.

cross-correlation function between observed PC1 (PDO type) and PC2 (NPGO type) of JFM SSTa (Figure 3a) exhibits a maximum of $R = 0.27$ (99% significance level) when PC2 leads PC1 by 1 year. When computing a sliding 20 year of the 1 year lead correlation coefficient between PC2 and PC1 over the period 1950–2013 (Figure 3b) we find a significant positive trend (>95% significance) with correlation reaching $R = 0.6$ over the last 30 years (the 2014/2015 events were excluded as outliers because of their large size). This increase in correlation is evident in both the NOAA ERSSTv3 and HadiSST reanalysis and suggests a strong increase in the multiyear winter persistence of the North Pacific SSTa associated to recurrent patterns of decadal variability, namely, the NPGO (year 0) and PDO (year +1) type. An interesting aspect of this sliding correlation analysis is the negative values prior to 1950 (Figure 3b). While these values could be attributed to noise (e.g., significant correlations on periods of 20 years need to exceed $R = 0.4$), they may also suggest that the observed state contains a wider range of coupling dynamics between winter and winter SSTa than can lead to a negative coupling between PC2 (year 0) and PC1 (year +1). However, further analysis of the CESM-LENS (Figure S7d, discussed in the next section) shows that negative lag 1 year correlations never occur between PC2/PC1 in any of the ensemble members over the entire length of the simulations 1920–2100. This indicates that the lead-lag dynamics between the two dominant modes are very robust in the CESM-LENS and may suggest that the observational SSTa prior to 1950 may be inadequate (e.g., because of the under sampling) to fully resolve this type of variability.

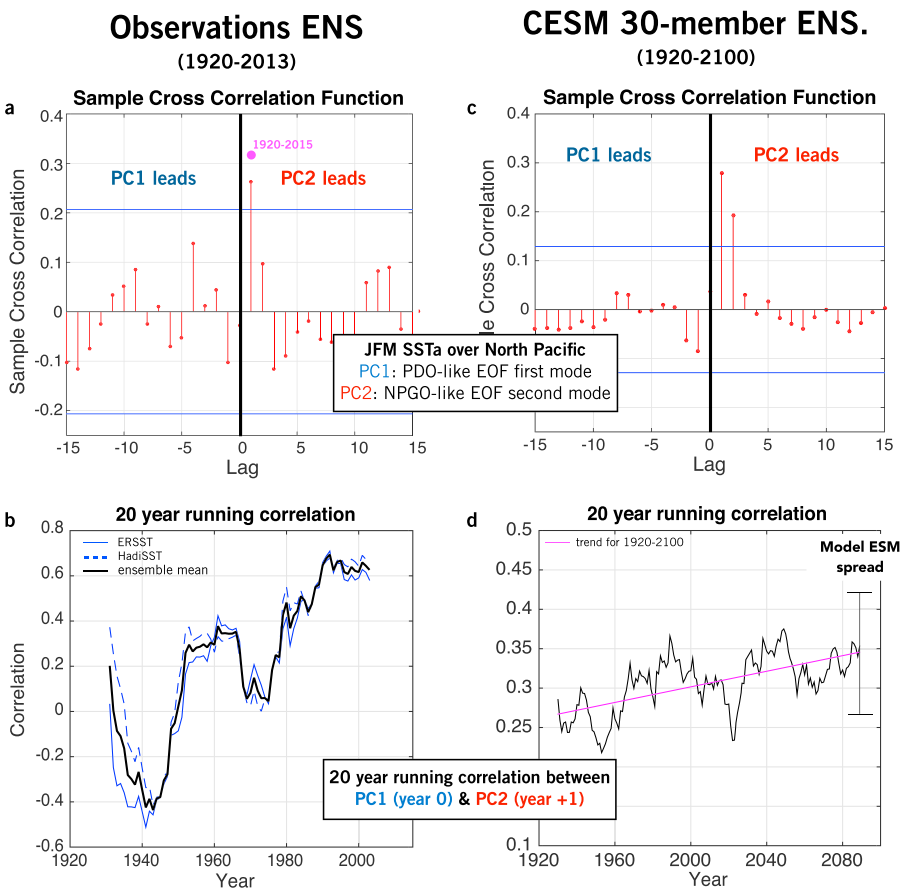

Figure 3. Joint statistics of the two Principal Components of NEP JFM SSTa in the observation ensemble and in the CESM-LENS 30-member ensemble. (a) Cross-correlation function of observations (ERSST and HadiSST) between observed PC1 and PC2 with a peak ($R = 0.27$, >95% significance) when the PC2 (NPGO type) leads PC1 (PDO type) by 1 year. The pink dot indicates a peak ($R = 0.32$, > 99% significance) when computing the same analysis using the period of 1920–2015. (b) One year lead relationship between observed PC2 with PC1 as a sliding 20 year correlation in the ERSSTv3 (blue line), HadiSST (blue dash line), and their ensemble mean (black line). (c) Cross-correlation function of CESM-LENS ensemble mean between PC1 and PC2 with a peak ($R = 0.28$, >95% significance) when the PC2 leads PC1 by 1 year. (d) Sliding 20 year correlation of ensemble mean of 1 year lead relationship between PC2 with PC1 with the model spread denoted as a gray bar. The pink line indicates a linear trend of 20 year running correlations in the period of 1920–2100 showing the slope of 0.08 with 94% confidence. The significance associated with lag-1 cross correlation of 30-member CESM having a positive relationship between PC2 and PC1 is tested using a Monte Carlo approach (Figure S7).

To understand the significance of the increase in coupling and persistence of North Pacific SSTa in the context of climate change, we now examine the statistics of consecutive multiyear warm events in the CESM-LENS Historical (1951–2000) and RCP8.5 (2051–2100) simulations (Figure 4). We use the OEI (1°C threshold case) extracted for each ensemble member to construct the concurrent and the +1 year lag regression maps in SSTa and SLPa. Similar to the observational findings (Figure 2), both the Historical and RCP8.5 simulations show that the warm events of the NEP originate as an NPGO-like pattern in the SSTa (Figures 4a and 4e) and evolve to a PDO-like expression accompanying El Niño (Figures 4b and 4f, at lags of 1 year). The correspondence with observations is particularly remarkable if we compare the recent observed period 1984–2013 (Figures 2a and 2b) with the simulations for 2015–2100 using the RCP8.5 radiative forcings (Figures 4a and 4b). To better isolate the projected trends for future climate in the CESM-LENS, we examine the difference maps RCP8.5 minus Historical. Consistent with the recent observational trends, the difference maps at 0 year lag reveal a stronger SSTa in the North Pacific with an equatorward subtropical intensification of the warm anomalies (compare Figures 2i versus 4i) followed at 1 year lag by a clear strengthening of the El Niño signature along the equator (compare Figures 2j versus 4j). Inspection of the SLPa difference maps in both

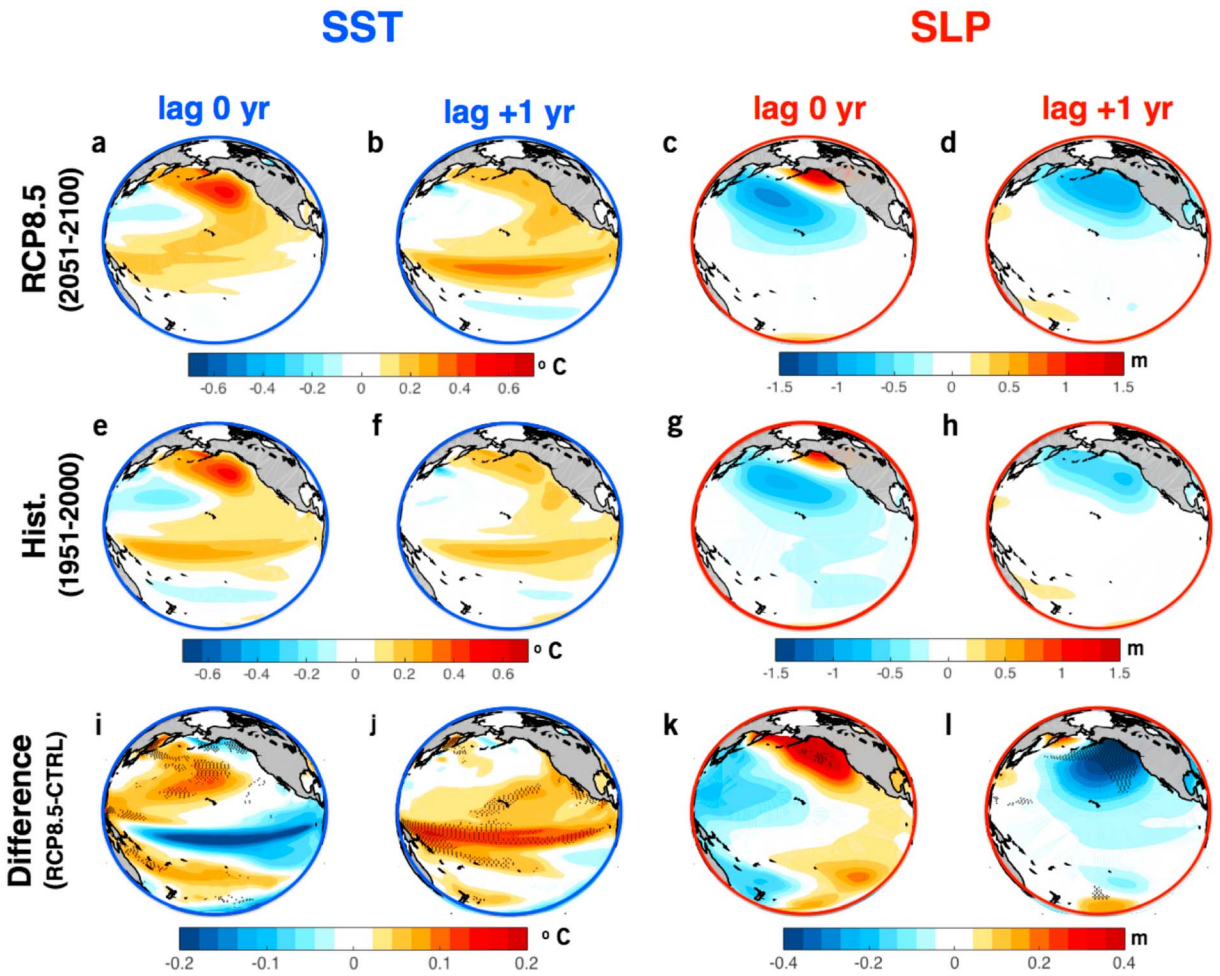

Figure 4. Evolution of the NEP warm events and related atmospheric forcing of the CESM-LENS ensemble mean. Regression maps of OEI (of 1°C) to SSTa and SLPa with 0 and +1 year lag for the 50 years of (a–d) RCP8.5 and (e–h) historical scenario. Difference maps between the (i–l) RCP8.5 and historical scenario (RCP8.5 minus historical). Stippling indicates regions where the difference of two regression coefficients is statistically significant above the 90% confidence level as determined by a two-tailed Student's *t* test.

observations and CESM-LENS (Figures 2k, 2l, 4k, and 4l) confirms that the SSTa trends are connected to a more prominent expression of the southern lobe of the NPO-like pattern at 0 year lag followed by deeper Aleutian Low at 1 year lag, which in the model is forced by the teleconnections induced by stronger El Niño SSTa in the tropics (Figures 2j and 4j). However, in CESM-LENS the strengthening of this teleconnection does not become apparent until the period 2051–2100. In fact, a comparison of regression maps between the two periods (1984–2013 versus 1951–1983 in Figure S8) in CESM-LENS exhibits no significant change. This indicates that the recent changes in the observations (Figure 2) cannot be attributed directly to anthropogenic-induced climate change, although they are consistent with the long-term response to anthropogenic warming (e.g., 2051–2100) as by the CESM-LENS.

The multiyear persistence of North Pacific SSTa in the CESM-LENS is quantified through the multimember ensemble 1 year lag cross correlation between PC2 (NPGO type) and PC1 (PDO type) (Figure 3c). We confirm that the model clearly captures the multiyear persistence of warm anomalies associated with the transition from an NPGO to PDO type patterns, with the 1 year lead correlation (PC2 versus PC1) $R = 0.28$ comparable to the observations $R = 0.27$ (Figure 3a). Similar to what is done for the two reanalysis data sets, we compute a sliding 20 year average of the 1 year lead correlation between PC2 and PC1 (Figure 3d) in each simulation to quantify the trends in coupling of the multiyear persistence. The CESM-LENS exhibits a positive trend ~35% increase in correlation (from $R = 0.27$ to $R = 0.35$) over the period 1920–2100, with 21 out of 30 simulations

showing a positive sign in the trend consistent with observations (Figure 3b). The model also shows a large spread around the ensemble mean (gray bar in Figure 3d) suggesting that the strong observed trend falls within the statistics of individual model realizations. Finally, we note that every ensemble members exhibits a positive correlation in the 1 year lag coupling between PC2 and PC1, even when considering windows of 20 years (Figure S7d). This confirms that the coupling between NPGO and PDO is a very robust dynamical feature of North Pacific climate variability in the CESM simulations.

5. Implications for Future Climate and Ecology

Taken together, these analyses suggest that the recent observational trends in the coupling between the NPGO and PDO-type patterns associated with the winter to winter persistence of warm anomalies in the NEP are consistent with future projections of climate change as inferred from the CESM-LENS RCP8.5 simulations in 2051–2100. However, a direct attribution of the recent trends to anthropogenic forcing is premature based on the CESM-LENS simulations, which show that these trends become statistically significant ~2050. The model simulations also suggest that NEP marine heatwaves will become larger in size (~18%) and amplitude (0.3–0.5°C) with the potential of strong and prolonged stresses on marine ecosystems in this region.

The physiological stress from the increasing persistence and magnitude of marine heatwaves might become an important driver altering a marine food webs in the NEP via range shifts of different species and corresponding shifts in ecosystem community structure (Munday et al., 2008; Tittensor et al., 2010; Wernberg et al., 2013). Widespread and extreme negative impacts on marine life and fisheries associated with the 2014–2015 marine heat wave are well documented. If the projected increases in the area, magnitude and frequency of extreme warm events are realized, and they are superimposed upon a systematic anthropogenic warming trend; this combination would likely cause profound negative impacts on marine life and fisheries all along the west coast of North America, particularly those in the Gulf of Alaska in the second half of the 21st century.

Acknowledgments
We acknowledge the support of the NSF-Easm 3506J16 and NSF-OCE 132022 and National Center for Atmospheric Research for producing and making available climate model data which is 30 members of the CESM-LENS, http://www.cesm.ucar.edu/projects/community-projects/LENS/data-sets.html. Observational SST data were obtained from https://www.esrl.noaa.gov/psd/data/gridded/data.noaa.ersst.v3.html (ERSSTv3) and https://www.metoffice.gov.uk/hadobs/hadisst/data/download.html (HadISST). The authors also thank Nate Mantua and two anonymous reviewers for constructive comments that significantly improved the manuscript.

References

Alexander, M. A. (1992). Midlatitude atmosphere ocean interaction during El Niño. 1. The North Pacific-Ocean. *Journal of Climate*, *5*(9), 944–958. https://doi.org/10.1175/1520-0442(1992)005%3C0944:maiden%3E2.0.co;2

Anderson, B. T., Gianotti, D. J., Furtado, J. C., & Di Lorenzo, E. (2016). A decadal 326 precession of atmospheric pressures over the North Pacific. *Geophysical Research Letters*, *43*, 3921–3927. https://doi.org/10.1002/2016GL068206

Anderson, B. T., Perez, R. C., & Karspeck, A. (2013). Triggering of El Niño onset through trade wind-induced charging of the equatorial Pacific. *Geophysical Research Letters*, *40*, 1212–1216. https://doi.org/10.1002/grl.50200

Baxter, S., & Nigam, S. (2015). Key role of the North Pacific Oscillation-West 280 Pacific pattern in generating the extreme 2013/14 North American Winter. *Journal of Climate*, *28*(20), 8109–8117. https://doi.org/10.1175/jcli-d-14-00726.1

Bond, N. A., Cronin, M. F., Freeland, H., & Mantua, N. (2015). Causes and impacts of the 2014 warm anomaly in the NE Pacific. *Geophysical Research Letters*, *42*, 3414–3420. https://doi.org/10.1002/2015GL063306

Chhak, K. C., Di Lorenzo, E., Schneider, N., & Cummins, P. F. (2009). Forcing of 337 low-frequency ocean variability in the Northeast Pacific. *Journal of Climate*, *22*(5), 1255–1276. https://doi.org/10.1175/2008jcli2639.1

Di Lorenzo, E., Liguori, G., Schneider, N., Furtado, J. C., Anderson, B. T., & Alexander, M. A. (2015). ENSO and meridional modes: A null hypothesis for Pacific climate variability. *Geophysical Research Letters*, *42*, 9440–9448. https://doi.org/10.1002/2015GL066281

Di Lorenzo, E., & Mantua, N. (2016). Multi-year persistence of the 2014/15 North Pacific marine heatwave. *Nature Climate Change*, *6*(11), 1042–1047. https://doi.org/10.1038/nclimate3082

Di Lorenzo, E., Schneider, N., Cobb, K. M., Franks, P. J. S., Chhak, K., Miller, A. J., … Rivière, P. (2008). North Pacific Gyre Oscillation links ocean climate and ecosystem change. *Geophysical Research Letters*, *35*, L08607. https://doi.org/10.1029/2007GL032838

Hartmann, D. L. (2015). Pacific sea surface temperature and the winter of 2014. *Geophysical Research Letters*, *42*, 1894–1902. https://doi.org/10.1002/2015GL063083

Hobday, A. J., Alexander, L. V., Perkins, S. E., Smale, D. A., Straub, S. C., Oliver, E. C. J., … Wernberg, T. (2016). A hierarchical approach 301 to defining marine heatwaves. *Progress in Oceanography*, *141*, 227–238. https://doi.org/10.1016/j.pocean.2015.12.014

Kay, J. E., Deser, C., Phillips, A., Mai, A., Hannay, C., Strand, G., … Vertenstein, M. (2015). The Community Earth System Model (CESM) large ensemble project: A community resource for studying climate change in the presence of internal climate variability. *Bulletin of the American Meteorological Society*, *96*, 1333–1349. https://doi.org/10.1175/BAMS-D-13-00255.1

Linkin, M. E., & Nigam, S. (2008). The north pacific oscillation-west Pacific teleconnection pattern: Mature-phase structure and winter impacts. *Journal of Climate*, *21*(9), 1979–1997. https://doi.org/10.1175/2007jcli2048.1

Mantua, N. J., Hare, S. R., Zhang, Y., Wallace, J. M., & Fracis, R. C. A. (1997). Pacific interdecadal climate oscillation with impacts on salmon production. *Bulletin of the American Meteorological Society*, *78*(6), 1069–1079. https://doi.org/10.1175/1520-0477

Munday, P. L., Jones, G. P., Pratchett, M. S., & Williams, A. J. (2008). Climate change and the future for coral reef fishes. *Fish and Fisheries*, *9*, 261–285.

Penland, C., & Sardeshmukh, P. D. (1995). The optimal-growth of tropical sea-surface temperature anomalies. *Journal of Climate*, *8*(8), 1999–2024. https://doi.org/10.1175/1520-0442(1995)008%3C1999:togots%3E2.0.co;2

Peterson, W., Bond, N., & Robert, M. (2016). The blob (part three): Going, going, gone? *PICES Press*, *24*, 46–48.

Rayner, N. A., Parker, D. E., Horton, E. B., Folland, C. K., Alexander, L. V., Rowell, D. P., … Kaplan, A. (2003). Global analyses of sea surface temperature, sea ice, and night marine air temperature since the late nineteenth century. *Geophysical Research Letters*, *108*(D14), 4407. https://doi.org/10.1029/2002JD002670

Smith, T. M., Reynolds, R. W., Peterson, T. C., & Lawrimore, J. (2008). Improvements NOAAs Historical Merged Land–Ocean Temp Analysis (1880–2006). *Journal of Climate*, *21*(10), 2283–2296. https://doi.org/10.1175/2007JCLI2100.1

Tittensor, D. P., Mora, C., Jetz, W., Lotze, H. K., Ricard, D., Berghe, E. V., & Worm, B. (2010). Global patterns and predictors of marine biodiversity across taxa. *Nature*, *466*(7310), 1098–1101. https://doi.org/10.1038/nature09329

Vimont, D. J., Wallace, J. M., & Battisti, D. S. (2003). The seasonal footprinting mechanism in the Pacific: Implications for ENSO. *Journal of Climate*, *16*(16), 2668–2675. https://doi.org/10.1175/1520-0442(2003)016%3C2668:tsfmit%3E2.0.co;2

Wang, S. Y., Hipps, L., Gillies, R. R., & Yoon, J. H. (2014). Probable causes of the abnormal ridge accompanying the 2013–2014 California drought: ENSO precursor and anthropogenic warming footprint. *Geophysical Research Letters*, *41*, 3220–3226. https://doi.org/10.1002/2014GL059748

Wernberg, T., Smale, D. A., Tuya, F., Thomsen, M. S., Langlois, T. J., de Bettigneis, T., … Rousseaux, C. S. (2013). An extreme climatic event alters marine ecosystem structure in a global biodiversity hotspot. *Nature Climate Change*, *3*, 78–82.